AAS 10-205

# FORTY-NINE BIASED STAR POSITIONS FROM ICESAT FLIGHT DATA

**Noah Smith,[*] Sungkoo Bae,[†] and Bob Schutz[‡]**

Approximately 1% of the 10,000 stars measured by the ICESat star trackers are believed to have position biases on the order of tens of arcseconds caused by near-neighbor stars. ICESat uses a Goodrich HD-1003 and two Ball CT-602 trackers. Empirical biases were derived for 49 stars, including four onboard catalog stars used by the Aura mission. A survey was performed to detect and characterize biased stars by treating each observed star as a target, predicting the tracker measurements of the target, and then comparing the observations and predictions. The distribution of prediction accuracies for unbiased stars had a mean of 1.46 arcseconds and a standard deviation of 0.61 arcseconds. 90% of the sky was covered and five million passes of 10,472 stars were processed. Stars were classified using a Mahalanobis distance parameter which scaled position residuals by prediction uncertainties. Stars with large Mahalanobis distances were then studied individually.

## INTRODUCTION

The ICESat star trackers are common models, a Goodrich HD-1003 and two Ball CT-602s. Approximately 1% of the 10,000 stars tracked are believed to have position biases on the order of tens of arcseconds. The biases are caused by unresolved near-neighbor stars that blend with the images of target stars.[1,3] This type of bias will continue to be a problem for future generations of star trackers. Higher angular resolution separates the images of neighboring stars, but the number and density of detectable stars increases rapidly with sensitivity. Biased positions are a problem for both star identification and attitude estimation because both methodologies compare observed and catalog positions. There are several descriptions in the literature of analytic methods for creating mission catalogs which are corrected for position biases.[4,5] This paper focuses on using flight data to estimate empirical mission catalog corrections.

Mission catalogs typically remove stars that are too faint or bright to be tracked and attempt to remove or correct stars with potential biases. The NASA SKY2000 Version 5 Master Catalog is the usual starting point for creating NASA mission catalogs. Astronomical missions using faint guide stars work directly with large astronomical catalogs. Some European missions work with the catalogs produced by the Hipparcos astrometry mission.[6] A table linking SKY2000 and Hipparcos identifiers was created for this project. SKY2000 Version 5 does not contain all of the stars typical trackers can acquire, or all of the near-neighbors that can effect target stars. The term

[*] Doctoral Candidate, Center for Space Research, University of Texas at Austin, USA
[†] Research Scientist/Engineer, Center for Space Research, University of Texas at Austin, USA
[‡] Professor and Associate Director, Center for Space Research, University of Texas at Austin, USA

"blended position" has been used for catalog records which represent the apparent centroid of a group of stars.[1,7] The SKY2000 catalog includes analytically derived blended positions for some near-neighbor cases. Records with blended positions are indicated by a binary flag.[8] Typical tracker image pixels cover about an arcminute of the sky and the star images are defocused to cover multiple pixels for centroiding with an accuracy of a few arcseconds. If a neighboring star is within a few arcminutes of a target star their light peaks overlap on the image pixels. The near-neighbor can alter the apparent centroid of the target and bias its measured position. Other types of bias besides static blended positions are possible. If the group members are intermittently resolved or include variable stars the blended position can vary with time, such cases have been called "ping-pong stars".[1,6] Analytic prediction of blended position centroids is difficult because of uncertainties in the instrument magnitudes of group members. The 2004 Aura mission catalog is of interest because of the work done on predicting near-neighbor effects (the results were later incorporated in the SKY2000 catalog). For the 3,542 stars in the Aura onboard catalog, near-neighbors within three arcminutes were analytically combined into blended positions based on the defocusing of Ball CT-602 type trackers. Of the 49 biased stars described in this paper, four appear in the Aura onboard catalog.

The NASA ICESat mission was launched on January 13, 2003 into a near-circular, frozen orbit with an altitude of approximately 600 km and an inclination of 94°. The science instrument is the Geoscience Laser Altimeter System (GLAS). ICESat carries four star trackers. The Instrument Star Tracker (IST) is a Raytheon Optical Systems, now Goodrich, HD-1003. It has an 8°×8° field of view, instrument magnitude 6.2 sensitivity, a 512×512 pixel CCD, and tracks up to 6 stars with 10 Hz sampling. The IST tracks any available stars in the field of view. The Laser Reference Sensor (LRS) is a second, modified 10 Hz HD-1003 with third-party optics and baffle reducing the field of view to 0.5°×0.5° and increasing the sensitivity to instrument magnitude 7.5. LRS data is not discussed in this paper due to its small field of view. GLAS also includes hemispherical resonating gyros sampled at 10 Hz. The two Ball Star Trackers (BST1 and BST2) are 10 Hz Ball CT-602 trackers pointing 30° to either side of the IST. The BSTs have an 8°×8° field of view, instrument magnitude 7.1 sensitivity, a 512×512 pixel CCD, and can track 5 stars simultaneously. The BSTs use position predicts from the flight computer to acquire stars specified in a mission catalog.[1,9]

## STAR TRACKER POSITION MEASUREMENTS AND ERRORS

A tracker coordinate frame is defined using three orthogonal axes with the *Z* axis along the optical axis and the *XY* axes in the image plane. The tracker attitude is the orientation of this frame with respect to the International Celestial Reference Frame (ICRF). A star is represented by a three-dimensional unit vector *u* pointing from the origin of the tracker frame. The unit vector representation is independent of tracker characteristics and is used when rotations are calculated, for example rotating a star catalog unit vector from the ICRF to a tracker coordinate frame.

Horizontal and vertical (*HV*) coordinates are also used to represent a star. They are expressed as a scaling of the tracker frame *XY* plane such that, at the center of the field of view, a unit of linear distance is equivalent to a one arcsecond change in direction of a star unit vector. One definition of *HV* coordinates uses the tracker focal length *f* and the *x* and *y* distances of the star image on the focal plane.

$$h = k\left(x/f\right) \tag{1}$$

$$v = k\left(y/f\right) \tag{2}$$

The scaling factor $k$ = 648000 arcseconds/π radians relates change of direction to distance. An equivalent definition of *HV* coordinates makes them independent of tracker characteristics by using similar triangles and the unit vector components.

$$h = k\left(u_1/u_3\right) \tag{3}$$

$$v = k\left(u_2/u_3\right) \tag{4}$$

Angular coordinates can be introduced. They are the output format of the Ball CT-602 star trackers.

$$\Theta_h = \tan^{-1}\left(u_1/u_3\right) = \tan^{-1}\left(h/k\right) \tag{5}$$

$$\Theta_v = \tan^{-1}\left(u_2/u_3\right) = \tan^{-1}\left(v/k\right) \tag{6}$$

The unit vector components have a simple expression in terms of the *HV* coordinates.

$$u_1'/1 = \tan\Theta_h = h/k \tag{7}$$

$$u_2'/1 = \tan\Theta_v = v/k \tag{8}$$

$$u' = \begin{bmatrix} u_1' & u_2' & 1 \end{bmatrix}^T \tag{9}$$

$$u = u'/\|u'\| \tag{10}$$

Tracker errors can be classified as low spatial frequency error, high spatial frequency error, and noise.[10] High spatial frequency error covers variations on the scale of the image pixels. For the ICESat trackers this is a 3 to 4 Hz zero-mean variation with amplitude of about an arcsecond and is not explicitly corrected. It may be useful to include a fourth class of tracker error for incorrect identification of target stars. Star identification is generally based on a search for a catalog star near an observed star.[11] For biased stars a better question may be: are there detectable stars near an observed star, and is there evidence that they caused the measurements? Another class of errors may be needed for timing, timestamp, and data gap issues.[12]

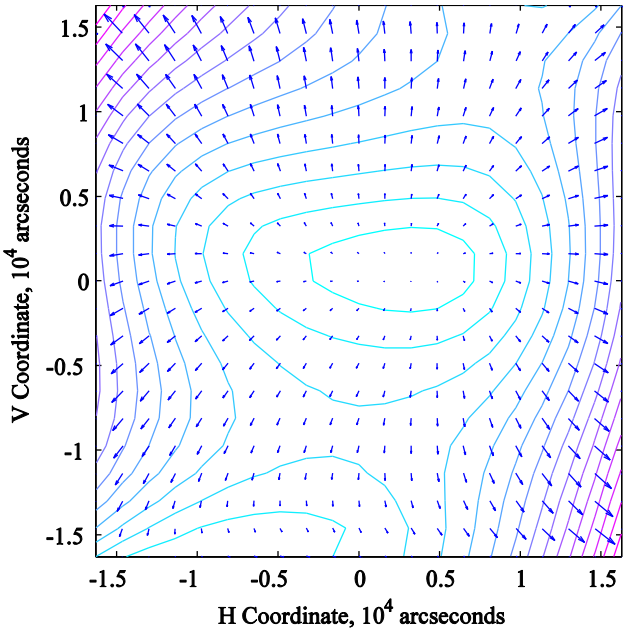


**Fig. 1 Low spatial frequency error corrections of up to 2.5 arcseconds for the IST field of view.**

Figure 1 shows the low spatial frequency error corrections for the IST. The corrections for BST1 and BST2 are similar. Low spatial frequency error includes position variations that occur on scales larger than the pixel size. Corrections for low spatial frequency errors were applied to all tracker measurements. These corrections were at most a few arcseconds. The corrections were estimated by fitting polynomials of the *HV* coordinates to the position errors.[13]

Noise estimation was based on the observed variations of the angular separations between pairs of stars.[14] The variance of the angular separation between two stars is equal to the sum of their individual angular variances. Given measurements of two stars, the variance of their angular separation can be calculated directly. For measurements of three stars, variances can be calculated for the angular separations of the three possible pairings of stars. Three equations can be formed and solved for the three unknown individual variances. When there are $n > 3$ stars, there can be a variable number $m$ of simultaneously measured pairs of stars and angular separations. If $m$ is greater than $n$, the resulting system of equations is over-determined and can be solved using least squares.

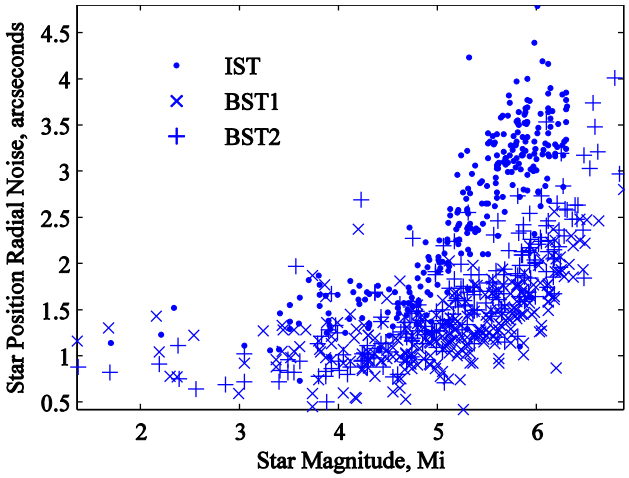


**Fig. 2 Radial position noise estimates versus star brightness.**

Figure 2 shows the estimated noise versus magnitude for the three trackers. The estimates are higher for the IST than for the other two trackers. They agree with the tracker performance statistics in the results section.

## BIASED STAR DETECTION

Using an iterative scheme, a segment of data was independently reprocessed for each star measured during the segment. Each star became the target star in turn. The set of measurements of the target star as it moved through the tracker field of view was defined as a star pass or simply pass. Measurements of the target star were set aside and tracker state estimation was performed using measurements of the other stars in the field of view during the pass. Predicted measurements for the target star were calculated using the tracker state estimates. Observed minus predicted position residuals and covariances were then calculated. Stars were classified using a parameter that scales the residuals by the covariances, indicating the statistical significance of the residuals.

Position covariances were estimated using attitude estimate covariances and the position noise of the target star. Attitude covariances were transformed from 3×3 matrices with units of radians-squared to 2×2 matrices with units of arcseconds-squared representing tracker *HV* coordinate uncertainties for the target star. The sensitivity matrix used in this transformation is derived here. The position measurement noise of the target star was estimated using the variations of the angles between pairs of simultaneously measured stars throughout the target star pass.

### Position Residual *r*

The target star observations, predictions, and covariances were expressed in a fixed coordinate frame where they could be directly compared. In the fixed frame both the observed and predicted positions were ideally constant. The predicted positions were a function of the fixed frame attitude and the star catalog position, so they were in fact constant. Errors in the observations and attitude estimates naturally produced variations of the observed positions. For each target star observation there was an estimated attitude defining a sample coordinate frame. These sample attitudes were estimated using the other stars observed by the tracker and excluding the target star. The fixed frame was arbitrary, but a specified sample attitude estimate from the middle of the target star pass was used in practice.

Each target star observation was first expressed as a unit vector in its sample coordinate frame. The sample frame was then rotated to the fixed frame while holding the observed unit vector constant in inertial space. The components of the unit vector were then recomputed relative to the fixed frame. The observation in the fixed frame for sample *i* and unit vector *u* was then expressed in *HV* coordinates.

$$p_i \equiv \begin{bmatrix} k(u_1/u_3) & k(u_2/u_3) \end{bmatrix}^T \tag{11}$$

The predicted position in the fixed frame was calculated similarly, giving the catalog unit vector of the target star relative to the fixed frame.

$$p_{predict} \equiv \text{star catalog position expressed in the fixed frame} \tag{12}$$

The position residual *r* was defined as the difference of the observed and predicted position.

$$r_i \equiv p_i - p_{predict} \tag{13}$$

The residual was expressed in *HV* coordinates with units that correspond to arcseconds near the center of the tracker field of view. The residuals for a target star pass clustered in a Gaussian distribution about zero, unless the star had a position bias.

**Position Covariance *S***

For each position residual, an *HV* coordinates 2×2 prediction covariance matrix *S* represented the position uncertainty. It was calculated as the sum of the 2×2 noise covariance *R* and the 3×3 attitude estimate covariance *P* transformed by a 2×3 sensitivity matrix *H*.

$$S = R + HPH^T \tag{14}$$

The measurement noise covariance *R* was the star position noise calculated as described above using pairs of stars. It was expressed in *HV* coordinates as a diagonal covariance matrix with units of arcseconds squared. The attitude estimate covariance *P* was calculated along with the attitude estimates using the SVD attitude estimation method, with observations weighted by noises. The sensitivity matrix *H* derived below was used to transform the attitude covariance *P* with units of radians squared to a covariance matrix in *HV* coordinates with units of arcseconds squared.

The sensitivity matrix *H* gave the change of a position residual *r* resulting from a perturbation of the estimated attitude. The attitude perturbation was a three-axis rotation $\delta\theta$.

$$\delta\theta = \begin{bmatrix} \delta\theta_1 & \delta\theta_2 & \delta\theta_3 \end{bmatrix}^T \tag{15}$$

For position residuals, it was equivalent to apply the perturbation to the fixed frame or to the sample frame attitude estimate. During the perturbation the observed star unit vector was held fixed. Multiplying the sensitivity matrix and the perturbation gave the small changes of the observed position vector $p_i$ and position residual $r_i$ .

$$\delta r_i = \delta p_i = H\delta\theta \tag{16}$$

The sensitivity matrix was formed by multiplying two matrices. The first matrix gave the change of the unit vector and the second gave the change of *HV* coordinates of the position residual. The matrix giving the change of the unit vector *u* was derived for the first two vector components, the third component was not needed.

$$\begin{bmatrix} \delta u_1 \\ \delta u_2 \end{bmatrix} = \begin{bmatrix} \partial u_1/\partial\theta_1 & \partial u_1/\partial\theta_2 & \partial u_1/\partial\theta_3 \\ \partial u_2/\partial\theta_1 & \partial u_2/\partial\theta_2 & \partial u_2/\partial\theta_3 \end{bmatrix}\Bigg|_{u_{10},u_{20}} \begin{bmatrix} \delta\theta_1 \\ \delta\theta_2 \\ \delta\theta_3 \end{bmatrix} \tag{17}$$

The unit vector components before the perturbation were $u_{10}$ and $u_{20}$ and the change $\delta u$ was the difference of the coordinates before and after the perturbation.

$$\delta u_1 \equiv u_1 - u_{10} \tag{18}$$

$$\delta u_2 \equiv u_2 - u_{20} \tag{19}$$

A rotation matrix for a 1-2-3 rotation sequence was used to derive expressions for $\delta u_1$ and $\delta u_2$.

$$\begin{bmatrix} u_1 \\ u_2 \\ u_3 \end{bmatrix} = \begin{bmatrix} c\theta_2 c\theta_3 & c\theta_1 s\theta_3 + s\theta_1 s\theta_2 c\theta_3 & s\theta_1 s\theta_3 - c\theta_1 s\theta_2 c\theta_3 \\ -c\theta_2 s\theta_3 & c\theta_1 c\theta_3 - s\theta_1 s\theta_2 s\theta_3 & s\theta_1 c\theta_2 + c\theta_1 s\theta_2 s\theta_3 \\ s\theta_2 & -s\theta_1 c\theta_2 & c\theta_1 c\theta_2 \end{bmatrix} \begin{bmatrix} u_{10} \\ u_{20} \\ u_{30} \end{bmatrix} \tag{20}$$

The change of the first unit vector component was derived by substituting in the small angles perturbation $\delta\theta$.

$$u_1 = \left(c\delta\theta_2 c\delta\theta_3\right)u_{10} + \left(c\delta\theta_1 s\delta\theta_3 + s\delta\theta_1 s\delta\theta_2 c\delta\theta_3\right)u_{20} + \left(s\delta\theta_1 s\delta\theta_3 - c\delta\theta_1 s\delta\theta_2 c\delta\theta_3\right)u_{30} \tag{21}$$

$$u_1 = u_{10} + \left(\delta\theta_3 + \delta\theta_1\delta\theta_2\right)u_{20} + \left(\delta\theta_1\delta\theta_3 - \delta\theta_2\right)u_{30} \tag{22}$$

$$\delta u_1 = \begin{bmatrix} 0 & -u_{30} & u_{20} \end{bmatrix}\delta\theta \tag{23}$$

The change of the second unit vector component was derived in the same way.

$$u_2 = (-c\delta\theta_2 s\delta\theta_3)u_{10} + (c\delta\theta_1 c\delta\theta_3 - s\delta\theta_1 s\delta\theta_2 s\delta\theta_3)u_{20} + \left(s\delta\theta_1 c\delta\theta_2 + c\delta\theta_1 s\delta\theta_2 s\delta\theta_3\right)u_{30} \tag{24}$$

$$u_2 = (-\delta\theta_3)u_{10} + (1 - \delta\theta_1\delta\theta_2\delta\theta_3)u_{20} + \left(\delta\theta_1 + \delta\theta_2\delta\theta_3\right)u_{30} \tag{25}$$

$$\delta u_2 = \begin{bmatrix} u_{30} & 0 & -u_{10} \end{bmatrix}\delta\theta \tag{26}$$

The two components were combined to form the sub-matrix giving $\delta u$ the change of the first two components of the unit vector $u$.

$$\begin{bmatrix} \delta u_1 \\ \delta u_2 \end{bmatrix} = \begin{bmatrix} 0 & -u_{30} & u_{20} \\ u_{30} & 0 & -u_{10} \end{bmatrix} \begin{bmatrix} \delta\theta_1 \\ \delta\theta_2 \\ \delta\theta_2 \end{bmatrix} \tag{27}$$

The matrix giving the change of *HV* coordinates of the position residual was derived from the equations for the *HV* representation of tracker observations.

$$h \equiv f_h(u) = k\left(u_1/u_3\right) \tag{28}$$

$$v \equiv f_v(u) = k\left(u_2/u_3\right) \tag{29}$$

The change of the *H* component was derived from the Taylor series expression.

$$h(u) = h(u_0) + \left.\frac{\partial f_h}{\partial u}\right|_{u_0} (u - u_0) + \ldots \tag{30}$$

$$\delta h = \left[ k/u_3 + ku_1^2/u_3^3 \quad ku_1u_2/u_3^3 \right]_{u_0} \delta u \tag{31}$$

The change of the *V* component was derived in the same way.

$$v(u) = v(u_0) + \left.\frac{\partial f_v}{\partial u}\right|_{u_0} (u - u_0) + \ldots \tag{32}$$

$$\delta v = \left[ ku_1u_2/u_3^3 \quad k/u_3 + ku_2^2/u_3^3 \right]_{u_0} \delta u \tag{33}$$

Multiplying the change of *HV* coordinates with the change of the unit vector gave the sensitivity matrix.

$$H = \begin{bmatrix} k/u_3 + ku_1^2/u_3^3 & ku_1u_2/u_3^3 \\ ku_1u_2/u_3^3 & k/u_3 + ku_2^2/u_3^3 \end{bmatrix} \begin{bmatrix} 0 & -u_3 & u_2 \\ u_3 & 0 & -u_1 \end{bmatrix} \tag{34}$$

This expression for the sensitivity matrix was evaluated using the observed unit vector expressed in the fixed frame.

**Mahalanobis Distance *d***

The variation of position residuals was described empirically by their distribution in *HV* coordinates and analytically by their *S* matrices. For a sample of *n* position residuals with the same covariance *S*, their sample distribution was Gaussian by the central limit theorem and their sample distribution covariance decreased with the square root of the sample size *n*.

$$\text{sample distribution covariance} = S/\sqrt{n} \tag{35}$$

This was demonstrated by plots of position residuals, examples are shown in the results section. As the sample size increased the distributions of residuals formed narrower and sharper peaks on the *HV* plane. This principle of reducing positional uncertainty by increasing the sample size is important in astrometry.[15]

To classify a star as biased, its position residuals and covariances were considered together. A useful scalar parameter that combined *r* and *S* was the Mahalanobis distance *d*.

$$d^2 = r^T S^{-1} r \tag{36}$$

The parameter *d* was viewed as a ratio of the position residual and the position uncertainty. Position residuals with large uncertainties had smaller *d* values. Experience showed that *d* values greater than 1 to 1.5 indicated a significant position bias.

## SURVEY CHARACTERISTICS

Public ICESat data available from the National Snow and Ice Data Center (NSIDC) were used for the survey. This limited sky coverage to ICESat laser campaigns. The campaigns were approximately 33 days long. The identifiers for the campaigns used were: 2a, 2c, 3b, 3f, 3g, and 3h (2a was about 45 days long). In total they covered 228 days from 2003 to 2007.

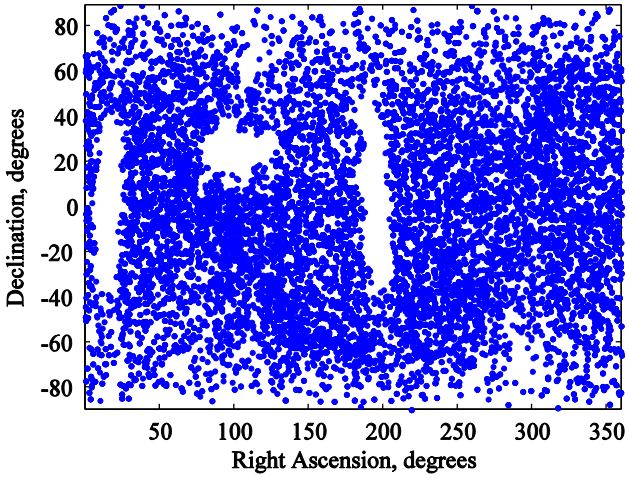


**Fig. 3 Stars found in the survey.**

Figure 3 shows the survey sky coverage. 90% of the sky was covered and five million passes of stars through tracker fields of view were processed. The nodes of the ICESat orbit plane moved about 0.5° per day or 180° per year. The sun was near the orbit plane during campaigns 2c and 3f, creating the hole in coverage at 100° right ascension in Fig. 3. The two vertical gaps at 20° and 200° right ascension are areas that were not covered by the selected survey data (since only campaign data were used, if data from between campaigns were added these holes should be filled).

The mean length of a pass of a star through a field of view was 78.3 ± 27.7 seconds. Passes less than 10 seconds long were edited out because of small sample sizes. his also rejected some unusual cases such as transients (satellites, dust particles) mistaken for stars or biased stars that were only marginally being identified. After editing, the survey data included 3.4 million passes of 10,472 unique stars.

**Table 1 Numbers of unique stars found in the survey grouped by tracker**

| Tracker | Number of stars | Exclusive | IST | BST1 | BST2 | All |
|---|---|---|---|---|---|---|
| IST | 9410 | 4903 | - | 244 | 391 | 3872 |
| BST1 | 4755 | 267 | 244 | - | 292 | 3872 |
| BST2 | 4978 | 305 | 391 | 292 | - | 3872 |

Table 1 shows the numbers of unique stars found in the survey, grouped by tracker. The IST measured any star in its field of view, resulting in a larger number of IST stars than BST stars. The BSTs operated in directed mode, measuring stars as directed by the flight computer. The

flight computer used an onboard attitude estimate and catalog of selected stars to direct the BST virtual trackers where to acquire new stars.

Two levels of statistics were computed: pass statistics for every pass of a star through a tracker field of view, and star statistics for every star based on its pass statistics. One version of star statistics was computed using all three trackers, and three additional versions used each tracker alone. Estimated biases were effectively the same for all three trackers. This was not surprising considering all three trackers had the same basic characteristics of field of view and pixel size. The most significant differences between the trackers were sensitivity and noise and their overall effect on star biases was small. The statistics and plots in the results section are for all three trackers unless noted. For a star that was observed in *n* passes there were *n* pass statistics for position residuals *r* and Mahalanobis distances *d*.

$$r_i,\ i = 1,...,n \tag{37}$$

$$d_i,\ i = 1,...,n \tag{38}$$

Star statistics for $r$ and $d$ were defined as the median values of the pass statistics.

$$r = median\left(r_1,...,r_n\right) \tag{39}$$

$$d = median\left(d_1,...,d_n\right) \tag{40}$$

Median values were used to reduce the effects of outliers. Two criteria were used to classify a star as unbiased: if the star statistics for $r$ and $d$ were less than five arcseconds and one. If a star did not meet these criteria, indicating there was not sufficient evidence that it was unbiased, it was marked for additional investigation.

## RESULTS

The survey results are descriptions of 49 biased stars, and statistics for thousands of unbiased stars. Biased stars are given in two tables: the first lists 45 stars, the second lists four stars in the Aura mission onboard catalog. Six pairs of astronomical images and residual plots demonstrate that near-neighbors cause the biases.

Statistics for unbiased stars characterize the overall error. The complete process from tracker observations to position predictions is treated as a black box. Unbiased stars are used as inputs to the black box and statistics describing the output are used to evaluate its performance. The first table shows significant differences in performance between the trackers. Another table relates performance with star brightness. Three tables are grouped by sample time and show little evidence of tracker aging effects over the five years covered by the survey data.

### Biased Stars

Once a biased star was detected, its position residual was converted to astronomical right ascension and declination coordinates for comparison with astronomical images. Lines of right ascension converge on the poles and away from the equator right ascension residuals become large compared to declination residuals. Right ascension residuals were multiplied by the cosine of the star declination to make the scaling of both residuals similar. For the absolute location of a biased star on the sky, the right ascension residual must be divided by the cosine of the star declination.

**Table 2 Biased stars found in the survey**

| SKYMAP | HIP | Dec. | Passes | BST passes | *d* | R.A. residual × cos(Dec.) (arcseconds) | Dec. residual (arcseconds) |
|---|---|---|---|---|---|---|---|
| 8190190 | 40817 | -71.5 | 598 | - | 11.50 ± 0.64 | 26.43 ± 1.39 | 18.05 ± 2.19 |
| 21570079 | 108378 | 66.1 | 224 | 2 | 9.41 ± 1.79 | -20.99 ± 1.60 | 16.63 ± 5.10 |
| 21430083 | 107253 | 38.3 | 36 | 15 | 9.29 ± 2.45 | 23.82 ± 6.41 | 14.35 ± 2.46 |
| 21440193 | 107382 | -9.1 | 108 | - | 9.26 ± 0.74 | -10.42 ± 0.90 | 24.96 ± 1.44 |
| 21020031 | 103814 | -43.0 | 415 | - | 9.18 ± 0.30 | 24.68 ± 1.51 | 7.36 ± 0.47 |
| 110134 | 967 | 48.2 | 145 | 14 | 8.74 ± 0.88 | 16.88 ± 1.53 | 19.39 ± 0.94 |
| 14240025 | 70400 | 5.8 | 280 | 21 | 8.39 ± 0.59 | -23.90 ± 1.15 | 1.69 ± 0.65 |
| 16200091 | 80047 | -78.7 | 1925 | 7 | 7.06 ± 0.54 | 3.95 ± 1.80 | 19.85 ± 1.10 |
| 22220131 | 110478 | -46.0 | 513 | 169 | 6.88 ± 2.36 | 20.52 ± 6.61 | 7.50 ± 2.79 |
| 20180172 | 100122 | 35.0 | 57 | 9 | 6.19 ± 1.20 | -7.19 ± 2.23 | 22.79 ± 3.57 |
| 9570131 | 48839 | -1.9 | 493 | 296 | 5.02 ± 0.84 | 14.79 ± 1.52 | -4.06 ± 1.20 |
| 21440030 | 107310 | 28.7 | 269 | 14 | 4.52 ± 0.51 | 8.88 ± 1.25 | 10.62 ± 1.23 |
| 15240088 | 75411 | 37.4 | 215 | - | 4.43 ± 0.42 | 1.22 ± 0.79 | -12.69 ± 0.45 |
| 310089 | 2484 | -63.0 | 880 | 880 | 4.30 ± 0.62 | -3.14 ± 0.54 | 12.91 ± 1.00 |
| 14130055 | 69481 | 51.8 | 1331 | 931 | 3.77 ± 0.54 | 9.27 ± 0.98 | 6.15 ± 0.98 |
| 2540010 | 13518 | -50.9 | 1076 | 756 | 3.69 ± 0.77 | 3.07 ± 1.69 | 10.79 ± 3.10 |
| 16400088 | 81632 | -20.4 | 280 | 36 | 3.66 ± 0.69 | -9.06 ± 2.22 | 5.27 ± 1.57 |
| 21420079 | 107162 | 41.1 | 10 | - | 3.64 ± 0.38 | 8.78 ± 1.25 | -4.63 ± 1.06 |
| 3230087 | 15795 | 58.7 | 50 | 36 | 3.36 ± 0.47 | -9.16 ± 1.25 | 2.79 ± 1.53 |
| 16160102 | 79757 | 29.2 | 348 | 274 | 3.32 ± 0.82 | 6.54 ± 2.49 | 6.33 ± 1.15 |
| 20220229 | 100515 | 43.0 | 43 | 1 | 3.23 ± 0.37 | 8.75 ± 1.24 | 3.47 ± 0.37 |
| 18560046 | 92946 | 4.2 | 26 | - | 3.17 ± 0.20 | 8.68 ± 0.65 | -2.59 ± 0.37 |
| 18490160 | 92391 | -5.9 | 118 | 29 | 3.07 ± 0.49 | 2.73 ± 1.14 | -8.56 ± 1.09 |
| 21010039 | 103734 | 36.0 | 1044 | 645 | 2.71 ± 0.68 | 5.51 ± 1.80 | 5.93 ± 2.23 |
| 4110075 | 19571 | -20.4 | 377 | 273 | 2.66 ± 0.46 | -3.02 ± 1.58 | 7.21 ± 1.29 |
| 21440054 | 107323 | -55.5 | 1786 | 1317 | 2.53 ± 0.44 | 7.42 ± 1.21 | 0.49 ± 1.34 |
| 14260028 | 70574 | -45.2 | 144 | 84 | 2.52 ± 0.60 | -3.09 ± 1.27 | -6.89 ± 1.85 |
| 4500154 | 22534 | -53.5 | 117 | 2 | 2.49 ± 0.62 | -5.05 ± 1.88 | -4.10 ± 2.20 |
| 22550117 | 113222 | 36.4 | 277 | 180 | 2.43 ± 0.51 | -6.72 ± 1.22 | -3.62 ± 1.89 |
| 9510120 | 48374 | -46.6 | 1468 | 1223 | 2.28 ± 0.27 | -0.80 ± 0.85 | 6.78 ± 0.58 |
| 19240223 | 95447 | 11.9 | 249 | 249 | 2.28 ± 0.37 | -6.38 ± 0.95 | 1.70 ± 0.97 |
| 9290031 | 46509 | -2.8 | 319 | 218 | 2.23 ± 0.21 | 1.10 ± 0.98 | 6.30 ± 0.55 |
| 22080173 | 109332 | -18.5 | 478 | 471 | 2.11 ± 0.56 | 3.57 ± 1.29 | 5.00 ± 1.41 |
| 16080010 | 79043 | 17.1 | 261 | 26 | 2.09 ± 0.28 | 1.61 ± 0.72 | 6.07 ± 0.64 |
| 13510003 | 67589 | 68.3 | 1287 | 881 | 2.03 ± 0.51 | 5.73 ± 1.09 | 2.59 ± 0.92 |
| 17340102 | 85998 | 9.6 | 289 | 1 | 2.03 ± 0.38 | -0.45 ± 1.60 | -5.86 ± 1.06 |
| 20000063 | 98461 | -37.7 | 186 | 186 | 1.97 ± 0.37 | 4.53 ± 0.97 | -4.48 ± 0.74 |
| 20370024 | 101716 | 26.5 | 201 | 163 | 1.90 ± 0.54 | 5.20 ± 1.67 | 1.69 ± 0.68 |
| 10550078 | - | 24.8 | 794 | 533 | 1.87 ± 0.24 | -4.70 ± 0.81 | 2.40 ± 0.60 |

| | | | | | | | |
|---|---|---|---|---|---|---|---|
| 14190049 | 69996 | -46.1 | 1232 | 1104 | 1.85 ± 0.45 | 2.08 ± 0.78 | -4.93 ± 1.23 |
| 21190179 | - | -53.5 | 2158 | 1705 | 1.82 ± 0.34 | 5.16 ± 1.02 | -0.20 ± 0.85 |
| 19290088 | 95823 | -43.5 | 67 | 67 | 1.81 ± 0.15 | 4.12 ± 0.40 | 2.89 ± 0.24 |
| 9010159 | 44342 | 27.9 | 213 | 213 | 1.80 ± 0.28 | -6.71 ± 2.03 | 1.50 ± 0.96 |
| 11270140 | 55945 | 2.9 | 598 | 411 | 1.79 ± 0.29 | -0.08 ± 0.95 | -5.34 ± 0.71 |
| 19150063 | 94624 | 15.1 | 262 | 262 | 1.79 ± 0.25 | -5.07 ± 0.78 | -0.41 ± 0.66 |

Table 2 describes 45 biased stars. The first two columns contain SKYMAP and Hipparcos identifiers. SKYMAP identifiers are also SKY2000 identifiers (the SKY2000 catalog is a later version of the SKYMAP catalog). The third column contains star declinations for calculating absolute right ascension residuals by dividing using the cosine of the declination. The passes column contains the number of passes and pass-level statistics which were combined in the star-level statistics. The BST passes column is of interest because the BSTs are in directed mode and only track stars in an onboard mission catalog. The last three columns contain the star-level statistics: Mahalanobis distances, right ascension residuals, and declination residuals. The star-level statistics are the median values and standard deviations of the distributions of pass-level statistics. Astronomical images from the SIMBAD database showed near-neighbors for each of these stars. Plots of right ascension and declination residuals confirmed that the directions and magnitudes of the residuals correlated with the positions of the near-neighbors. Example astronomical images and residual plots are given for the first two stars (the two stars with the largest Mahalanobis distances) in Figs. 4 and 5.

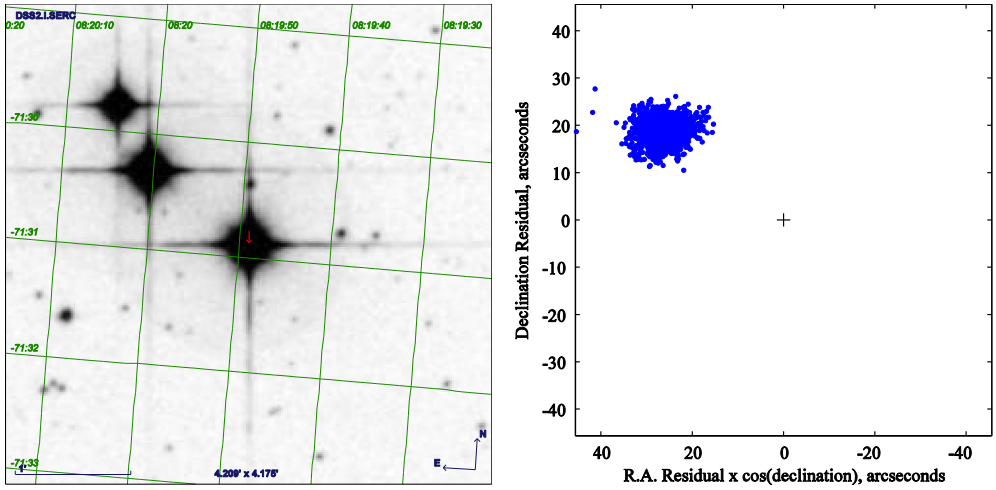


**Fig. 4 SKYMAP 8190190, 240" × 240" astronomical image (left) and observed minus predicted residual plot (right).**

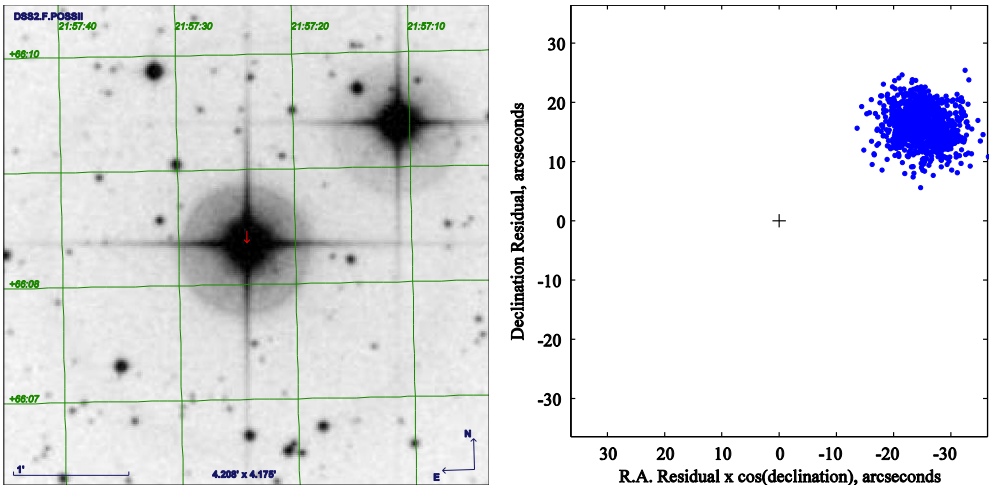


**Figure 5. SKYMAP 21570079, 240" × 240" astronomical image (left) and observed minus predicted residual plot (right).**

Figures 4 and 5 are astronomical images and residual plots for the first two stars in Table 2. The cross in the center of the residuals plots is the predicted position. The scattered points are the observed positions relative to the predicted position. The right ascension residuals have been scaled by the cosine of the star declination so that the axes scales are similar.

**Table 3 Biased stars found in the survey that are also in the Aura onboard catalog**

| SKYMAP | HIP | Aura | Dec. | Passes | BST passes | *D* | R.A. residual × cos(Dec.) (arcseconds) | Dec. residual (arcseconds) |
|---|---|---|---|---|---|---|---|---|
| 23190077 | 115152 | 3025 | 48.6 | 238 | - | 15.51 ± 1.46 | 29.65 ± 1.92 | 34.99 ± 1.31 |
| 17310145 | 85786 | 759 | -33.7 | 77 | - | 8.28 ± 1.75 | 17.76 ± 4.33 | -17.05 ± 4.09 |
| 14290104 | 70874 | 20 | -76.7 | 959 | 565 | 3.33 ± 0.91 | -8.99 ± 1.81 | 2.88 ± 2.67 |
| 19370139 | 96536 | 1204 | -14.3 | 144 | 144 | 2.74 ± 0.38 | 3.07 ± 0.74 | -7.70 ± 1.25 |

Table 3 describes four biased stars that are also in the Aura onboard catalog. The 2004 Aura mission catalog is of special interest because of the work done on near-neighbors, particularly for the 3542 stars in the Aura onboard catalog. The third column contains the Aura onboard catalog identifier. Astronomical images and residual plots are given for these four stars in Figs. 6-9.

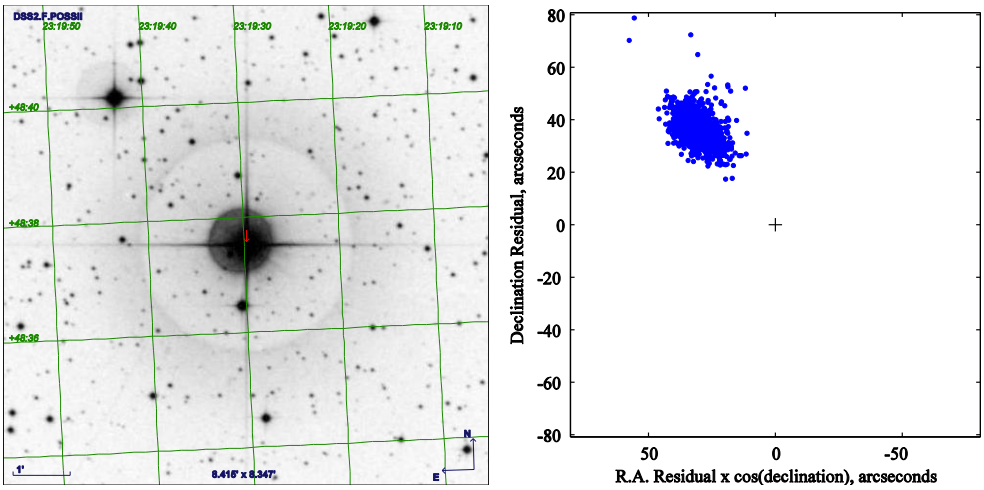


**Figure 6. SKYMAP 23190077 Aura 3025, 300" × 300" astronomical image (left) and observed minus predicted residual plot (right).**

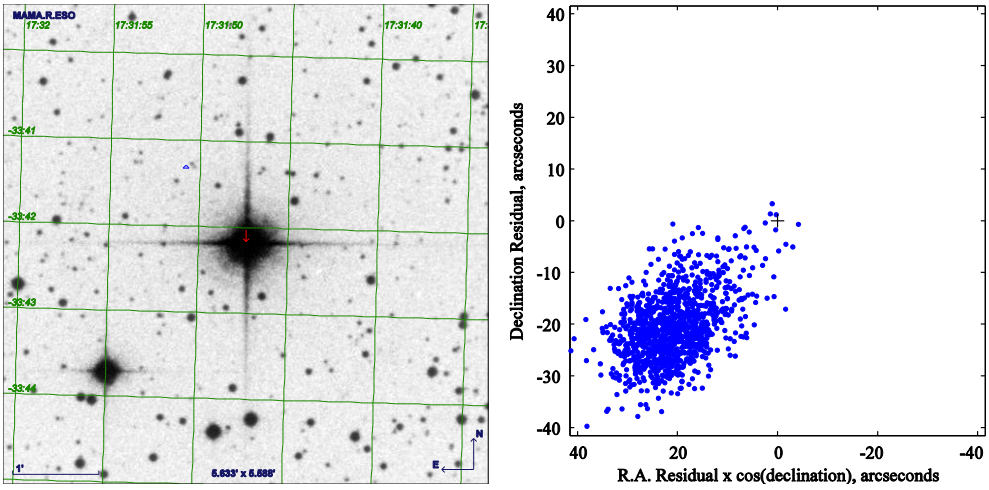


**Figure 7. SKYMAP 17310145 Aura 759, 300" × 300" astronomical image (left) and observed minus predicted residual plot (right).**

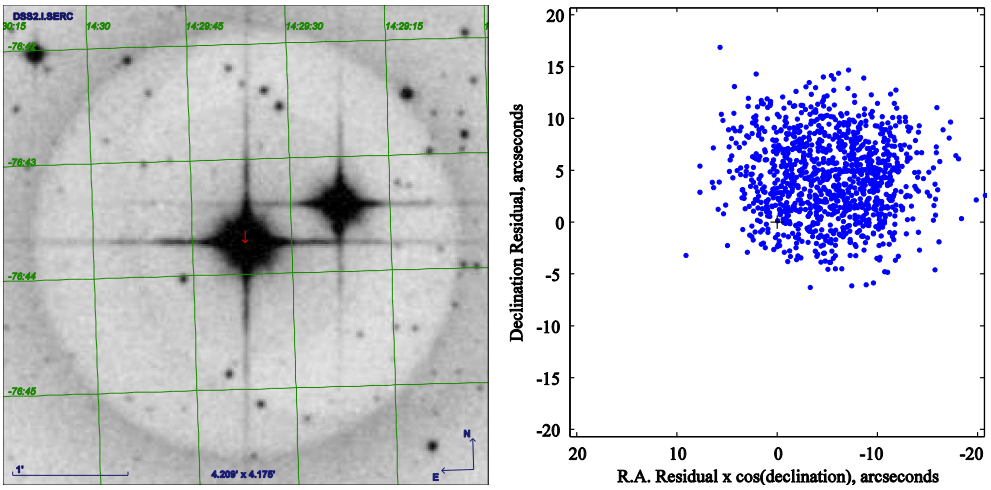


**Figure 8. SKYMAP 14290104 Aura 70874, 240" × 240" astronomical image (left) and observed minus predicted residual plot (right).**

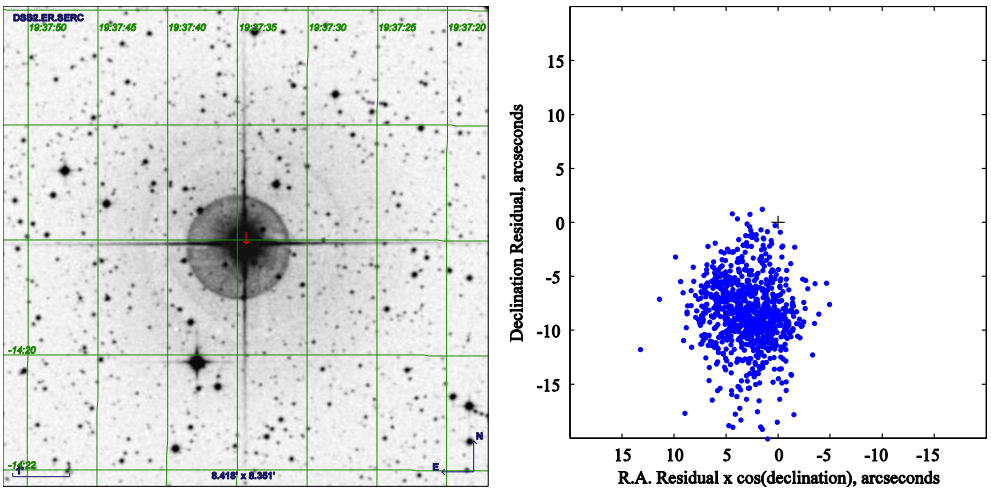


**Figure 9. SKYMAP 19370139 Aura 1204, 300" × 300" astronomical image (left) and observed minus predicted residual plot (right).**

## Unbiased Stars

Unbiased stars had position residuals less than five arcseconds and Mahalanobis distances less than one. Statistics for large samples of unbiased stars were used to characterize the trackers. The samples were selected by tracker, by star brightness, and by observation time. The statistics combined the effects of measurement errors and prediction errors. They described the complete process of tracker observations and model predictions. The distributions of position residuals $r$ and Mahalanobis distances $d$ were described using mean values and standard deviations. The criteria defining unbiased stars meant that the distributions were roughly Gaussian by the central limit theorem. The distributions of passes per star $n$ were also described using mean values, though $n$ is far from Gaussian. Many bright stars were tracked during every possible pass, while many dim stars were tracked in a handful of the possible passes. The two extremes dominated. The result was that the standard deviation of $n$ was generally larger than its mean.

**Table 4 Position residual statistics for unbiased stars grouped by tracker**

| Tracker | Stars | Mean passes *n* | *r* (arcseconds) | *d* |
|---|---|---|---|---|
| IST | 4894 | 210.1 | 1.63 ± 0.62 | 0.54 ± 0.19 |
| BST1 | 4378 | 234.6 | 1.20 ± 0.62 | 0.39 ± 0.20 |
| BST2 | 4217 | 248.9 | 1.37 ± 0.64 | 0.46 ± 0.21 |
| All | 6187 | 513.7 | 1.46 ± 0.61 | 0.49 ± 0.20 |

Table 4 contains statistics for unbiased stars grouped by tracker. BST1 had smaller position residuals than the other two trackers. This quantitative result agreed with other qualitative evidence. The position residual $r$ was treated as the overall accuracy of the system. Ideally it would be zero. The error described by this statistic comes from both the tracker measurements and the prediction process.

**Table 5 Position residual statistics for unbiased stars grouped by star brightness**

| Star Mi | Stars | Mean passes *n* | *r* (arcseconds) | *d* |
|---|---|---|---|---|
| 1 to 2 | 20 | 926.3 | 1.39 ± 0.78 | 0.47 ± 0.25 |
| 2 to 3 | 99 | 658.0 | 1.44 ± 0.60 | 0.47 ± 0.19 |
| 3 to 4 | 361 | 635.4 | 1.44 ± 0.65 | 0.48 ± 0.21 |
| 4 to 5 | 1028 | 637.3 | 1.34 ± 0.62 | 0.45 ± 0.19 |
| 5 to 6 | 2889 | 516.2 | 1.47 ± 0.63 | 0.49 ± 0.20 |
| 6 to 7 | 2792 | 252.1 | 1.56 ± 0.65 | 0.51 ± 0.20 |

Table 5 shows statistics grouped by star magnitude. Position residuals generally increased with magnitude. This agreed with the increase of position noise with magnitude shown in Figure 2. The number of stars increased with magnitude because of the increase of star density with faintness. More passes of bright stars were observed indicating that the trackers acquired fainter stars less frequently.

**Table 6 IST position residual statistics grouped by campaign**

| Campaign | Stars | Mean passes *n* | *r* (arcseconds) | *d* |
|---|---|---|---|---|
| L2A 2003 | 1398 | 181.5 | 1.52 ± 0.61 | 0.50 ± 0.19 |
| L2C 2004 | 1010 | 146.5 | 1.65 ± 0.62 | 0.54 ± 0.19 |
| L3B 2005 | 1075 | 152.7 | 1.66 ± 0.63 | 0.53 ± 0.19 |
| L3F 2006 | 1025 | 147.5 | 1.70 ± 0.61 | 0.57 ± 0.20 |
| L3G 2006 | 1276 | 119.3 | 1.60 ± 0.70 | 0.53 ± 0.21 |
| L3H 2007 | 1386 | 111.0 | 1.59 ± 0.67 | 0.52 ± 0.21 |

**Table 7 BST1 position residual statistics grouped by campaign**

| Campaign | Stars | Mean passes *n* | *r* (arcseconds) | *d* |
|---|---|---|---|---|
| L2A 2003 | 1365 | 199.2 | 1.22 ± 0.65 | 0.40 ± 0.21 |
| L2C 2004 | 913 | 139.8 | 1.16 ± 0.67 | 0.38 ± 0.21 |
| L3B 2005 | 1146 | 153.8 | 1.23 ± 0.62 | 0.40 ± 0.20 |
| L3F 2006 | 743 | 158.1 | 1.26 ± 0.67 | 0.41 ± 0.21 |
| L3G 2006 | 1280 | 126.3 | 1.22 ± 0.65 | 0.40 ± 0.21 |
| L3H 2007 | 1464 | 111.3 | 1.22 ± 0.65 | 0.40 ± 0.21 |

**Table 8 BST2 position residual statistics grouped by campaign**

| Campaign | Stars | Mean passes *n* | *r* (arcseconds) | *d* |
|---|---|---|---|---|
| L2A 2003 | 1365 | 193.8 | 1.37 ± 0.67 | 0.44 ± 0.22 |
| L2C 2004 | 987 | 142.3 | 1.40 ± 0.65 | 0.46 ± 0.21 |
| L3B 2005 | 1063 | 168.4 | 1.40 ± 0.65 | 0.47 ± 0.21 |
| L3F 2006 | 839 | 159.1 | 1.41 ± 0.66 | 0.47 ± 0.21 |
| L3G 2006 | 1193 | 129.3 | 1.41 ± 0.66 | 0.48 ± 0.22 |
| L3H 2007 | 1389 | 117.0 | 1.36 ± 0.67 | 0.46 ± 0.23 |

Tables 6-8 characterize the distributions of $r$ and $d$ for each tracker during the six laser campaigns used in the survey. Tracker aging effects could have caused variations of the statistics over time. The laser campaigns were taken from the first five years of the mission. There was not strong evidence of aging effects.

## CONCLUSION

Attitude and pointing estimation depend on accurate measurements of star unit vectors in the tracker coordinate frame, and on accurate star catalog unit vectors in the ICRF. The star position biases estimated here from ICESat flight data are systematic errors in the measurements, but they can also be viewed as errors in knowledge of the star catalog unit vectors. In effect, the apparent sky for the trackers is different than the sky described by the star catalogs. The empirical position biases correct the star catalog to accurately describe the apparent sky, improving star identification and attitude estimation. The method described here is to use an initial sky catalog to predict what a tracker will see, and then use differences between observations and predictions to correct the catalog to more accurately describe the apparent sky. It is applicable to future generations of star trackers. As tracker sensitivity increases the number and density of detectable near-neighbor stars increases rapidly. Better angular resolution and estimation of the apparent sky are necessary for continuous increases of overall attitude and pointing accuracy.

## ACKNOWLEDGMENTS

This research has made use of the SIMBAD database, operated at CDS, Strasburg, France. It has also made use of the JPL On-Line Solar System Data Service.

## REFERENCES


[1] R. A. Fowell, N. Smith, S. Bae, B. E. Schutz, "Bad Stars." 32nd AAS GN&C Conference, Breckenridge Colorado, Advances in the Astronautical Sciences, Vol. 133, pp. 20-36, 2009. URL: https://webspace.utexas.edu/noahsmit/papers/AAS09012.pdf (Archived by WebCite® at http://www.webcitation.org/5eUBJ3BY1)

[2] B. McCutcheon, "FHST Near Neighbor Problems and Integrated Magnitude Spoilers." STScI Report, 2000. URL: http://tinyurl.com/lgtsqn Accessed: 2009-09-17 (Archived by WebCite® at http://www.webcitation.org/5bcctue8Z).

[3] C. Sande, G. Natanson, D. Tracewell, "Effects of Uncataloged Near-Neighbor Stars on CCDST Operation." Flight Mechanics Symposium, Goddard Space Flight Center, Maryland, 2005. URL: http://tinyurl.com/l6rd84 Accessed: 2009-09-17 (Archived by WebCite® at http://www.webcitation.org/5bcnXSzuI).

[4] R. W. H. Van Bezooijen, L. Degen, H. Nichandros, "Guide Star Catalog for the Spitzer Space Telescope Pointing Calibration and Reference Sensor." Optical, Infrared, and Millimeter Space Telescopes, Proceedings of the SPIE, Vol. 5487, pp. 253-265, 2004.

[5] P. Kudva, A. Throckmorton, "Preliminary star catalog development for the Earth Observation System AM1 (EOS-AM1) mission." *Journal of Guidance, Control, and Dynamics*. Vol. 19, No. 6, 1996, pp. 1332-1336.

[6] M. Lauer, "Operational Experience with Autonomous Star Trackers on ESA Interplanetary Spacecraft." 20th International Symposium on Space Flight Dynamics, Annapolis, MD, NASA-CP-2007-214158, 2007. URL: http://www.webcitation.org/5bsHH711r Accessed: 2009-09-17 (Archived by WebCite® at http://www.webcitation.org/5bsHH711r)

[7] D. Mortari, J. L. Junkins, M. A. Samaan, "Lost-In-Space Pyramid Algorithm for Robust Star Pattern Recognition." Breckenridge, CO, Advances in the Astronautical Sciences, Vol. 107, pp. 49-68, 2001.

[8] C. Sande, N. Ottenstein, "SKYMAP Requirements, Functional, and Mathematical Specifications." Computer Sciences Corporation Report, CSC-96-932-24, 1999. URL: http://tinyurl.com/m29vsj Accessed: 2009-09-17. (Archived by WebCite® at http://www.webcitation.org/5jrOOwX4o)

[9] B. E. Schutz, S. Bae, N. Smith, J. M. Sirota, "Precision Orbit And Attitude Determination For ICESat." F. Landis Markley Astronautics Symposium, Cambridge Maryland, Advances in the Astronautical Sciences, Vol. 132, 2008. URL: http://tinyurl.com/mbwbr8 Accessed: 2009-09-17 (Archived by WebCite® at http://www.webcitation.org/5eCDhyCAb)

[10] Y.-W. Wu, R. Li, "Star Tracker Error Characteristics and Their Compensation Techniques." NASA CP-2003-212246, 2003. URL: http://www.webcitation.org/5jkFYAUX5 Accessed: 2009-09-17 (Archived by WebCite® at http://www.webcitation.org/5jkFYAUX5)

[11] D. Mortari, "SP-search: A new algorithm for star pattern recognition." Advances in the Astronautical Sciences, Vol. 102, pp. 1165-1174, 1999.

[12] S. Bae, R. Ricklefs, N. Smith, B. E. Schutz, "Time Tag Issues in the Star Tracker and Gyro Data for ICESat Precision Attitude Determination." 19th AAS/AIAA Spaceflight Mechanics Meeting, Savannah Georgia, Advances in the Astronautical Society, Vol. 134, pp. 431-444, 2009. URL: http://tinyurl.com/nzq3sd Accessed: 2009-09-17 (Archived by WebCite® at http://www.webcitation.org/5eMYnoOfH)

[13] N. Smith, "Localized Distortion Estimation and Correction for the ICESat Star Trackers." M.S. Thesis Thesis, University of Texas, 2006. URL: http://tinyurl.com/kq9bev Accessed: 2009-09-17 (Archived by WebCite® at http://www.webcitation.org/5eCDpqvVP)

[14] M. Lauer, "Operational Experience with Autonomous Star Trackers on ESA Interplanetary Spacecraft." NASA CP-2007-214158, 2007. URL: http://www.webcitation.org/5bsHH711r Accessed: 2009-09-17 (Archived by WebCite® at http://www.webcitation.org/5bsHH711r)

[15] N. Zacharias, B. Dorland, "The Concept of a Stare-mode Astrometric Space Mission." *Publications of the Astronomical Society of the Pacific*. Vol. 118, No. 848, 2006, pp. 1419-1427.